Article

Flow towards a Stagnation Region of a Curved Surface in a Hybrid Nanofluid with Buoyancy Effects

Iskandar Waini [1,2], **Anuar Ishak** [2,*] and **Ioan Pop** [3]

1   Fakulti Teknologi Kejuruteraan Mekanikal dan Pembuatan, Universiti Teknikal Malaysia Melaka, Hang Tuah Jaya, Durian Tunggal 76100, Melaka, Malaysia; iskandarwaini@utem.edu.my

2   Department of Mathematical Sciences, Faculty of Science and Technology, Universiti Kebangsaan Malaysia, UKM Bangi 43600, Selangor, Malaysia

3   Department of Mathematics, Babeş-Bolyai University, 400084 Cluj-Napoca, Romania; ipop@math.ubbcluj.ro

*   Correspondence: anuar_mi@ukm.edu.my

Abstract: This paper examines the impact of hybrid nanoparticles on the stagnation point flow towards a curved surface. Silica (SiO_2) and alumina (Al_2O_3) nanoparticles are added into water to form SiO_2-Al_2O_3/water hybrid nanofluid. Both buoyancy-opposing and -assisting flows are considered. The governing partial differential equations are reduced to a set of ordinary differential equations, before being coded in MATLAB software to obtain the numerical solutions. Findings show that the solutions are not unique, where two solutions are obtained, for both buoyancy-assisting and -opposing flow cases. The local Nusselt number increases in the presence of the hybrid nanoparticles. The temporal stability analysis shows that only one of the solutions is stable over time.

Keywords: curved surface; hybrid nanofluid; mixed convection; heat transfer; stability analysis; stagnation point

1. Introduction

The phenomenon of the flow on a stagnation region commonly occurs in aerodynamic industries and engineering applications. To name a few, such applications are polymer extrusion, drawing of plastic sheets, and wire drawing. In some situations, the flow is stagnated by a solid wall, while in other cases a free stagnation point or line exists interior to the fluid domain. Historically, Hiemenz [1] was the first researcher to consider the boundary layer flow toward a stagnation point on a rigid surface. Moreover, the axisymmetric flow was considered by Homann [2], whereas the oblique flow was studied by Chiam [3]. Furthermore, Merkin [4] studied a similar problem by considering the mixed convection flow. He discovered that the solution is not unique for the opposing flow case. However, Ishak et al. [5] exposed that the dual solutions occur for both opposing and assisting flows. Several studies on the stagnation point flow subjected to various flow and physical conditions have been considered by the researchers for the past few years. For instance, the magnetohydrodynamic and the double stratification effects were examined by Khashi'ie et al. [6]. The unsteady flow was studied by Dholey [7] and Fang et al. [8]. The stagnation point viscoelastic fluid flow was examined by Mahapatra and Sidui [9]. Moreover, Weidman [10] investigated the porous medium effects, while the thermophoretic and Brownian diffusions were reported by Kumar et al. [11].

In 1995, Choi and Eastman [12] introduced the nanofluid, which is a mixture of the base fluid and a single type of nanoparticles, to enhance the thermal conductivity. The advantages of nanofluids in a rectangular enclosure have been reported by Khanafer et al. [13], Tiwari and Das [14], and Oztop and Abu-Nada [15]. Several researchers have published papers on nanofluids with various physical aspects, for example, magnetic field [16], viscous dissipation and chemical reaction [17], activation energy [18], Dufour and Soret [19],

magnetic dipole [20], and velocity slip [21]. For additional references, the experimental study on the nanoparticle's viscosity behavior can be found in refs. [22,23].

Recently, some studies have found that advanced nanofluid consists of another type of nanoparticle dispersed into the regular nanofluid could improve its thermal properties, and this mixture is termed as 'hybrid nanofluid'. Hybrid nanofluid is used to signal a promising increase in the thermal performance of working fluids since this technology has resulted in a significant change in the design of thermal and cooling systems. As a result of the addition of more types of nanostructures, a fluid with better thermal conductivity is created. Furthermore, hybrid nanofluids are used in several applications, for example, in the vehicle brake fluid, domestic refrigerator, solar water heating, transformer, and heat exchanger [24]. The earlier experimental works that using the hybrid nanoparticles were reported by Turcu et al. [25] and Jana et al. [26]. Moreover, Suresh et al. [27] conducted experimental works using Al_2O_3-Cu hybrid nanoparticles to study the enhancement of the fluid thermal conductivity. Moreover, the significance of the combination of Al_2O_3 and other nanoparticles was reported by Singh and Sarkar [28] and Farhana et al. [29]. The numerical studies on the hybrid nanofluid flow were studied by Takabi and Salehi [30]. In recent years, hybrid nanofluid was attracting the researcher's attention to study the flow and thermal behavior, numerically. For instance, the flow in the mini-channel heat sink was done by Kumar and Sarkar [31]. Meanwhile, the flow between two parallel plates with the squeezing effect was reported by Salehi et al. [32] and Muhammad et al. [33]. Apart from that, Waini et al. [34] and Khan et al. [35] considered the flow towards a shrinking surface. For further reading, the review papers on hybrid nanofluid can be found in Refs. [36–40].

It seems that Sajid et al. [41] were the first who studied the flow over a curved surface. They found that less drag force is required to move the fluid on a curved surface rather than that on a flat surface. Later, Sajid et al. [42] extended their work by considering a micropolar fluid. Since then, many researchers have continued the study of the flow and heat transfer induced by a curved surface under different conditions. For example, Abbas et al. [43] studied the curved stretching surface under the effect of the magnetic field in a viscous fluid, then later, they extended the problem with heat generation and thermal radiation effects in a nanofluid flow as reported in Abbas et al. [44]. Similarly, Hayat et al. [45], Imtiaz et al. [46], and Saba et al. [47] also reported the flow over a curved stretching surface in a nanofluid. Furthermore, Sanni et al. [48] and Hayat et al. [49] considered the nonlinear stretching velocity of the curved surface, while Okechi et al. [50] reported on the exponentially stretching curved surface. The unsteady flow was reported by Saleh et al. [51]. Naveed et al. [52] examined the dual solutions in hydromagnetic viscous fluid flow past a shrinking curved surface. Meanwhile, Khan et al. [53] explored the hybrid nanofluid flow with mixed convection. Based on the paper by Khan et al. [53], this paper aims to investigate the stagnation point flow of a hybrid nanofluid towards a curved surface containing Al_2O_3-SiO_2 nanoparticles with buoyancy effects. It should be mentioned that the condition of the surface temperature was assumed constant in Khan et al. [53]. In contrast to [53], the present paper considers the prescribed surface temperature case. Additionally, this paper examines the temporal stability of the numerical solutions.

2. Basic Equations

Consider the flow configuration model as shown in Figure 1. Here, the curved surface with radius R is measured about the curvilinear coordinates (r, s) where r is normal to tangent vector at any point on the sheet and s is the arc length coordinate along the flow direction, so that large values of R correspond to small curvature (slightly curved surface).
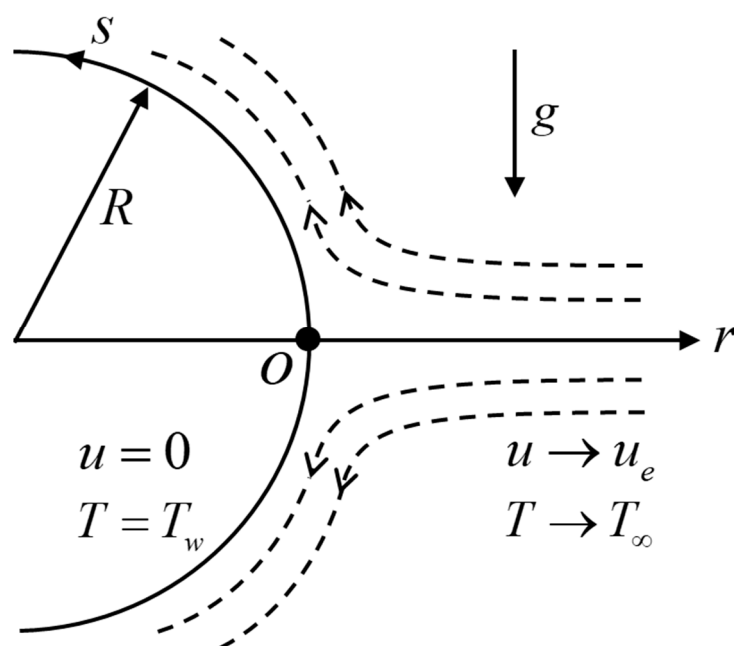
Figure 1. Flow configuration model of a curved surface.

According to Sajid et al. [41], the pressure is not constant across the boundary layer. Therefore, the pressure gradient in the case of a curved surface cannot be neglected. Here, it is supposed that $u_e(s) = as$ with $a > 0$ and $T_w(s) = T_\infty + T_0(s/L)$ where T_∞ is the constant ambient temperature, while T_0 and L, respectively, are the reference temperature and length. The prescribed surface temperature is employed to allow the similarity reduction of the equations. Considering hybrid nanofluid flow, a few assumptions are considered for the physical model. The hybrid nanofluid is assumed to be stable. Thus, the effect of nanoparticle aggregation and sedimentation is omitted. The nanoparticles are assumed to have a uniform size with a spherical shape. It is assumed that both the base fluid and nanoparticles are in a thermal equilibrium state, and they flow at the same velocity. Accordingly, under these assumptions along with the boundary layer approximations, the governing equations of hybrid nanofluid are [41,53]:

$$\frac{\partial}{\partial r}[(R+r)v] + R\frac{\partial u}{\partial s} = 0 \tag{1}$$

$$\frac{u^2}{R+r} = \frac{1}{\rho_{hnf}}\frac{\partial p}{\partial r} \tag{2}$$

$$v\frac{\partial u}{\partial r} + \frac{R}{R+r}u\frac{\partial u}{\partial s} + \frac{uv}{R+r} = -\frac{1}{\rho_{hnf}}\frac{R}{R+r}\frac{\partial p}{\partial s} + \frac{\mu_{hnf}}{\rho_{hnf}}\left(\frac{\partial^2 u}{\partial r^2} + \frac{1}{R+r}\frac{\partial u}{\partial r} - \frac{u}{(R+r)^2}\right) + \frac{(\rho\beta)_{hnf}}{\rho_{hnf}}(T - T_\infty)g \tag{3}$$

$$v\frac{\partial T}{\partial r} + \frac{R}{R+r}u\frac{\partial T}{\partial s} = \frac{k_{hnf}}{(\rho C_p)_{hnf}}\left(\frac{\partial^2 T}{\partial r^2} + \frac{1}{R+r}\frac{\partial T}{\partial r}\right) \tag{4}$$

subject to:

$$u = v = 0, \ T = T_w(s) \quad \text{at} \quad r = 0$$
$$u \to u_e(s), \ \frac{\partial u}{\partial r} \to 0, \ T \to T_\infty \quad \text{as} \quad r \to \infty \tag{5}$$

where v and u are the velocity components along r- and s- directions. Moreover, g and p are the acceleration caused by the gravity and the pressure, respectively, while the temperature is given by T. Furthermore, the thermophysical properties can be referred to in Tables 1 and 2 [30,53]. Please note that φ_1 (Al$_2$O$_3$) and φ_2 (SiO$_2$) are the nanoparticles

volume fractions where $\varphi_{hnf} = \varphi_1 + \varphi_2$, and the subscripts $n1$ and $n2$ are corresponded to their solid components, while the subscripts hnf and f signify the hybrid nanofluid and base fluid, respectively.

Table 1. Thermophysical properties of nanoparticles and water.

Properties	Base Fluid	Nanoparticles	
	Water	Al_2O_3	SiO_2
ρ (kg/m^3)	997.1	3970	2200
C_p (J/kgK)	4179	765	745
k (W/mK)	0.613	40	1.4
$\beta \times 10^{-5}$ (1/K)	21	0.85	42.7
Prandtl number, Pr	6.2		

Table 2. Thermophysical properties of hybrid nanofluid.

Properties	Correlations
Dynamic viscosity	$\mu_{hnf} = \dfrac{\mu_f}{\left(1-\varphi_{hnf}\right)^{2.5}}$
Density	$\rho_{hnf} = \left(1 - \varphi_{hnf}\right)\rho_f + \varphi_1\rho_{n1} + \varphi_2\rho_{n2}$
Heat capacity	$(\rho C_p)_{hnf} = \left(1 - \varphi_{hnf}\right)(\rho C_p)_f + \varphi_1(\rho C_p)_{n1} + \varphi_2(\rho C_p)_{n2}$
Thermal conductivity	$\dfrac{k_{hnf}}{k_f} = \dfrac{\frac{\varphi_1 k_{n1}+\varphi_2 k_{n2}}{\varphi_{hnf}}+2k_f+2(\varphi_1 k_{n1}+\varphi_2 k_{n2})-2\varphi_{hnf}k_f}{\frac{\varphi_1 k_{n1}+\varphi_2 k_{n2}}{\varphi_{hnf}}+2k_f-(\varphi_1 k_{n1}+\varphi_2 k_{n2})+\varphi_{hnf}k_f}$
Thermal expansion	$(\rho\beta)_{hnf} = \left(1 - \varphi_{hnf}\right)(\rho\beta)_f + \varphi_1(\rho\beta)_{n1} + \varphi_2(\rho\beta)_{n2}$

3. Similarity Transformations

Consider the similarity variables as in Sajid et al. [41]:

$$u = asf'(\eta), \; v = -\frac{R}{R+r}\sqrt{a v_f}f(\eta), \; p = \rho_f a^2 s^2 P(\eta), \; \theta(\eta) = \frac{T - T_\infty}{T_w - T_\infty}, \; \eta = r\sqrt{\frac{a}{v_f}} \quad (6)$$

where ($'$) signifies the differentiation with respect to η. Using Equation (6), the continuity equation, i.e., Equation (1) is identically fulfilled. Now, inserting Equation (6) in Equations (2) and (3), one obtains:

$$P' = \frac{\rho_{hnf}}{\rho_f}\frac{1}{K+\eta}f'^2 \quad (7)$$

$$\frac{\rho_f}{\rho_{hnf}}\frac{2K}{K+\eta}P = \frac{\mu_{hnf}/\mu_f}{\rho_{hnf}/\rho_f}\left(f''' + \frac{1}{K+\eta}f'' - \frac{1}{(K+\eta)^2}f'\right) + \frac{K}{(K+\eta)^2}ff' - \frac{K}{K+\eta}f'^2$$
$$+ \frac{K}{K+\eta}ff'' + \frac{(\rho\beta)_{hnf}/(\rho\beta)_f}{\rho_{hnf}/\rho_f}\lambda\theta \quad (8)$$

Then, the pressure P term in these equations is eliminated to obtain the following equation:

$$\frac{\mu_{hnf}/\mu_f}{\rho_{hnf}/\rho_f}\left(f^{iv} + \frac{2}{K+\eta}f''' - \frac{1}{(K+\eta)^2}f'' + \frac{1}{(K+\eta)^3}f'\right) + \frac{K}{K+\eta}\left(ff''' - f'f''\right) \quad (9)$$

Similarly, using Equation (6), Equation (4) is transformed to:

$$\frac{1}{Pr}\frac{k_{hnf}/k_f}{(\rho C_p)_{hnf}/(\rho C_p)_f}\left(\theta'' + \frac{1}{K+\eta}\theta'\right) + \frac{K}{K+\eta}\left(f\theta' - f'\theta\right) = 0 \quad (10)$$

subject to:

$$f(0) = 0, \quad f'(0) = 0, \quad \theta(0) = 1$$
$$f'(\infty) = 1, \quad f''(\infty) = 0, \quad \theta(\infty) = 0 \tag{11}$$

where $K = R\sqrt{a/\nu_f}$ (=constant) specifies the curvature parameter, ν_f represents the fluid kinematic viscosity, and $\Pr = \mu_f(C_p)_f/k_f$ represents the Prandtl number. Moreover, $\lambda = g\beta_f T_0/a^2 L = Gr_s/Re_s^2$ (=constant) represents the mixed convection or the buoyancy parameter, with $Gr_s = g\beta_f(T_w - T_\infty)s^3/\nu_f^2$ corresponds to the local Grashof number and $Re_s = u_e s/\nu_f$ stands for the local Reynolds number. Please note that $\lambda < 0$ signifies the opposing and $\lambda > 0$ signifies the assisting flows, while the forced convection flow (no buoyancy effects) is given by $\lambda = 0$.

The coefficient of the skin friction C_f and the local Nusselt number Nu_s are given as:

$$C_f = \frac{1}{\rho_f u_e^2} \mu_{hnf} \left(\frac{\partial u}{\partial r} - \frac{u}{R+r} \right)_{r=0}, \quad Nu_s = -\frac{s}{k_f(T_w - T_\infty)} k_{hnf} \left(\frac{\partial T}{\partial r} \right)_{r=0} \tag{12}$$

Using Equations (6) and (12), one gets:

$$Re_s^{1/2} C_f = \frac{\mu_{hnf}}{\mu_f} f''(0), \quad Re_s^{-1/2} Nu_s = -\frac{k_{hnf}}{k_f} \theta'(0) \tag{13}$$

Please note that by taking $\varphi_{hnf} = 0$ (regular fluid) and $K \to \infty$ (vertical plane surface), the problem reduces to the problem of Lok et al. [54] without the micropolar effects. Thus, the numerical values of $f''(0)$ and $-\theta'(0)$ can be validated with those obtained by them.

4. Stability Analysis

The temporal stability of the dual solutions as time evolves is studied. This analysis was first introduced by Merkin [55] and then followed by Weidman et al. [56]. First, consider the new variables as follows:

$$u = as\frac{\partial f}{\partial \eta}(\eta, \tau), \quad v = -\frac{R}{R+r}\sqrt{a\nu_f}\, f(\eta, \tau), \quad p = \rho_f a^2 s^2 P(\eta, \tau),$$
$$\theta(\eta, \tau) = \frac{T - T_w}{T_w - T_\infty}, \quad \eta = r\sqrt{\frac{a}{\nu_f}}, \quad \tau = at \tag{14}$$

Now, the unsteady form of Equations (3) and (4) are employed, while Equation (1) remains unchanged. On using (14), one obtains:

$$\frac{\mu_{hnf}/\mu_f}{\rho_{hnf}/\rho_f}\left(\frac{\partial^4 f}{\partial \eta^4} + \frac{2}{K+\eta}\frac{\partial^3 f}{\partial \eta^3} - \frac{1}{(K+\eta)^2}\frac{\partial^2 f}{\partial \eta^2} + \frac{1}{(K+\eta)^3}\frac{\partial f}{\partial \eta} \right) + \frac{K}{K+\eta}\left(f\frac{\partial^3 f}{\partial \eta^3} - \frac{\partial f}{\partial \eta}\frac{\partial^2 f}{\partial \eta^2} \right)$$
$$+ \frac{K}{(K+\eta)^2}\left(f\frac{\partial^2 f}{\partial \eta^2} - \left(\frac{\partial f}{\partial \eta}\right)^2 \right) - \frac{K}{(K+\eta)^3}f\frac{\partial f}{\partial \eta} + \frac{(\rho\beta)_{hnf}/(\rho\beta)_f}{\rho_{hnf}/\rho_f}\lambda\left(\frac{\partial \theta}{\partial \eta} + \frac{1}{K+\eta}\theta \right)$$
$$- \frac{1}{K+\eta}\frac{\partial^2 f}{\partial \eta \partial \tau} - \frac{\partial^3 f}{\partial \eta^2 \partial \tau} = 0 \tag{15}$$

$$\frac{1}{\Pr}\frac{k_{hnf}/k_f}{(\rho C_p)_{hnf}/(\rho C_p)_f}\left(\frac{\partial^2 \theta}{\partial \eta^2} + \frac{1}{K+\eta}\frac{\partial \theta}{\partial \eta} \right) + \frac{K}{K+\eta}\left(f\frac{\partial \theta}{\partial \eta} - \frac{\partial f}{\partial \eta}\theta \right) - \frac{\partial \theta}{\partial \tau} = 0 \tag{16}$$

subject to:

$$f(0, \tau) = 0, \quad \frac{\partial f}{\partial \eta}(0, \tau) = 0, \quad \theta(0, \tau) = 1$$
$$\frac{\partial f}{\partial \eta}(\infty, \tau) = 1, \quad \frac{\partial^2 f}{\partial \eta^2}(\infty, \tau) = 0, \quad \theta(\infty, \tau) = 0 \tag{17}$$

Then, consider the following perturbation functions [56]:

$$f(\eta, \tau) = f_0(\eta) + e^{-\gamma\tau}F(\eta), \quad \theta(\eta, \tau) = \theta_0(\eta) + e^{-\gamma\tau}G(\eta) \tag{18}$$

Here, Equation (18) is used to apply a small disturbance on the steady solution $f = f_0(\eta)$ and $\theta = \theta_0(\eta)$ of Equations (9)–(11). The functions $F(\eta)$ and $G(\eta)$ in Equation

(18) are relatively small compared to $f_0(\eta)$ and $\theta_0(\eta)$. The sign (positive or negative) of the eigenvalue γ determines the stability of the solutions. By employing Equation (18), Equations (15)–(17) become:

$$\frac{\mu_{hnf}/\mu_f}{\rho_{hnf}/\rho_f}\left(F^{iv} + \frac{2}{K+\eta}F''' - \frac{1}{(K+\eta)^2}F'' + \frac{1}{(K+\eta)^3}F'\right) + \frac{K}{K+\eta}\left(f_0 F''' + f_0''' F - f_0' F'' - f_0'' F'\right)$$
$$+ \frac{K}{(K+\eta)^2}\left(f_0 F'' + f_0'' F - 2f_0' F'\right) - \frac{K}{(K+\eta)^3}\left(f_0 F' + f_0' F\right) \qquad (19)$$
$$+ \frac{(\rho\beta)_{hnf}/(\rho\beta)_f}{\rho_{hnf}/\rho_f}\lambda\left(G' + \frac{1}{K+\eta}G\right) + \frac{\gamma}{K+\eta}F' + \gamma F'' = 0$$

$$\frac{1}{\text{Pr}}\frac{k_{hnf}/k_f}{(\rho C_p)_{hnf}/(\rho C_p)_f}\left(G'' + \frac{1}{K+\eta}G'\right) + \frac{K}{K+\eta}\left(f_0 G' + \theta_0' F - f_0' G - \theta_0 F'\right) + \gamma G = 0 \qquad (20)$$

subject to:

$$F(0) = 0, \quad F'(0) = 0, \quad G(0) = 0$$
$$F'(\infty) = 0, \quad F''(\infty) = 0, G(\infty) = 0 \qquad (21)$$

To obtain γ of Equations (19) and (20), the new boundary condition $F''(0) = 1$ is included in Equation (21) to replace $F''(\infty) = 0$.

5. Results and Discussion

Equations (9)–(11) are solved numerically by using the bvp4c function in MATLAB software (Matlab_R2014b, MathWorks, Singapore). As described in Shampine et al. [57], the aforesaid solver occupies a finite difference method that employs the 3-stage Lobatto IIIa formula. The selection of the initial guess and the boundary layer thickness, η_∞ is important to achieve the convergence of the numerical solution. This convergence issue is also influenced by the value of the physical parameters considered. The effects of several physical parameters on the flow and the thermal fields are investigated.

The values of $f''(0)$ and $-\theta'(0)$ for various λ when $\varphi_{hnf} = 0$ (regular fluid), $\text{Pr} = 0.7$ and $K \to \infty$ (plane surface) are compared with Lok et al. [54]. It is found that the results are comparable for each λ considered, as shown in Table 3. Moreover, the decreasing trend is observed in the first solution of $f''(0)$ and $-\theta'(0)$ for smaller values of λ. Furthermore, Table 4 provides the values of $Re_s^{1/2}C_f$ and $Re_s^{-1/2}Nu_s$ when $\text{Pr} = 6.2$ and $K = 10^3$ for numerous values of φ_{hnf} and λ. The consequence of rising φ_{hnf} exaggerates the values of $Re_s^{1/2}C_f$ and $Re_s^{-1/2}Nu_s$ for both branch solutions. Moreover, the values of $Re_s^{1/2}C_f$ are reduced as λ decreases for both branch solutions. Meanwhile, the values of $Re_s^{-1/2}Nu_s$ for the first solution are decreased with the decrease in λ, but they are increased for the second solution.

Table 3. Values of $f''(0)$ and $-\theta'(0)$ when $\varphi_{hnf} = 0$ (regular fluid), $\text{Pr} = 0.7$ and $K \to \infty$ for different λ.

| λ	Lok Et Al. [54]		Present Results	
	$f''(0)$	$-\theta'(0)$	$f''(0)$	$-\theta'(0)$
−1.0	0.691693	0.633269	0.691661	0.633247
			(−0.285049)	(−0.222165)
−1.5	0.371788	0.578230	0.371754	0.578206
	(−0.527666)	(−0.004360)	(−0.527651)	(−0.004347)
−2.0	−0.039513	0.486576	−0.039572	0.486540
	(−0.578523)	(0.198572)	(−0.578476)	(0.198599)

Results in "( )" are the lower branch (second) solutions.

Table 4. Values of $Re_s^{1/2}C_f$ and $Re_s^{-1/2}Nu_s$ when $K = 10^3$ and $\text{Pr} = 6.2$ for different physical parameters.

φ_{hnf}	λ	$Re_s^{1/2}C_f$		$Re_s^{-1/2}Nu_s$	
		First Solution	Second Solution	First Solution	Second Solution
2%	1	1.609474	0.652232	1.708511	2.232347
4%		1.684045	0.691249	1.759909	2.317150
6%		1.761695	0.731805	1.811141	2.401796
2%	−1	0.969496	−0.380839	1.530307	−1.239090
	−2	0.594987	−0.642901	1.403953	−0.295385
	−3	0.131804	−0.707488	1.208754	0.282748

Furthermore, the variations of $Re_x^{1/2}C_f$ and $Re_x^{-1/2}Nu_x$ against λ when $\text{Pr} = 6.2$ and $K = 10^3$ for various φ_{hnf} are presented in Figures 2 and 3. The enhancement in the values of $Re_x^{1/2}C_f$ and $Re_x^{-1/2}Nu_x$ are observed with a high percentage of the hybrid nanoparticle compositions. Moreover, the dual solutions are obtained for both opposing ($\lambda < 0$) and assisting ($\lambda > 0$) flows where the turning point of the solutions occurs in the opposing region ($\lambda < 0$). It is noticed that the critical values are $\lambda_c = -3.6169, -3.6219, -3.6270$ for $\varphi_{hnf} = 2\%, 4\%, 6\%$, respectively. Additionally, it is observed that the second solution of $Re_x^{1/2}C_f$ and $Re_x^{-1/2}Nu_x$ are undefined for non-buoyant case ($\lambda = 0$). From Figure 3, there exists an asymptotic line at $\lambda = 0$ where the second solutions of $Re_x^{-1/2}Nu_x$ show that the values of $Re_x^{-1/2}Nu_x \to +\infty$ as $\lambda \to 0^+$ and $Re_x^{-1/2}Nu_x \to -\infty$ as $\lambda \to 0^-$.

Moreover, Figures 4 and 5 display the profiles of $f'(\eta)$ and $\theta(\eta)$ when $\varphi_{hnf} = 2\%$, $\text{Pr} = 6.2$, and $K = 10^3$ for various values of λ. It is noticed that the profiles of the first and the second solutions are merged towards some values of λ. Additionally, a negative value ($\theta(\eta) < 0$) for the second solution of $\theta(\eta)$ is observed when $\lambda = 1$ and its gradient is greater than that of the first solution. Next, Figures 6 and 7 show the consequence of φ_{hnf} on $f'(\eta)$ and $\theta(\eta)$ when $\lambda = -1$, $\text{Pr} = 6.2$, and $K = 10^3$. It is seen that both branch solutions of $f'(\eta)$ show the decreasing pattern, whereas both branch solutions of $\theta(\eta)$ increases for a higher percentage of φ_{hnf}.
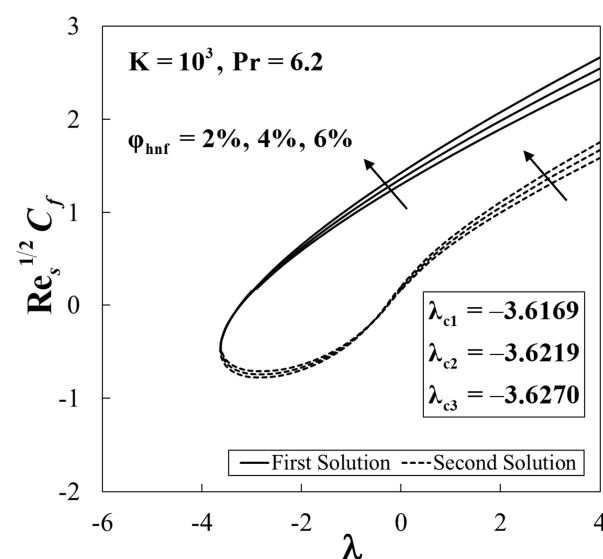
Figure 2. Variation of the skin friction coefficient $Re_s^{1/2}C_f$ against the mixed convection parameter λ for different values of φ_{hnf}.
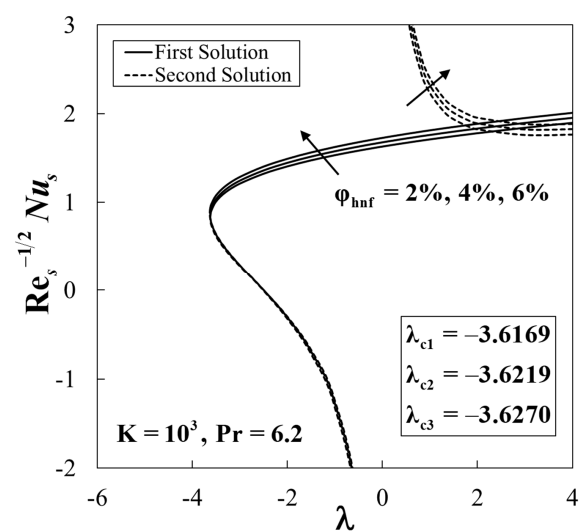
Figure 3. Variation of the local Nusselt number $Re_s^{-1/2}Nu_s$ against the mixed convection parameter λ for different values of φ_{hnf}.
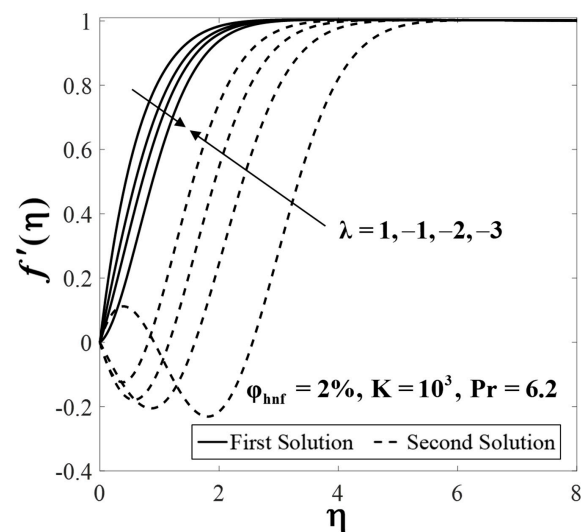

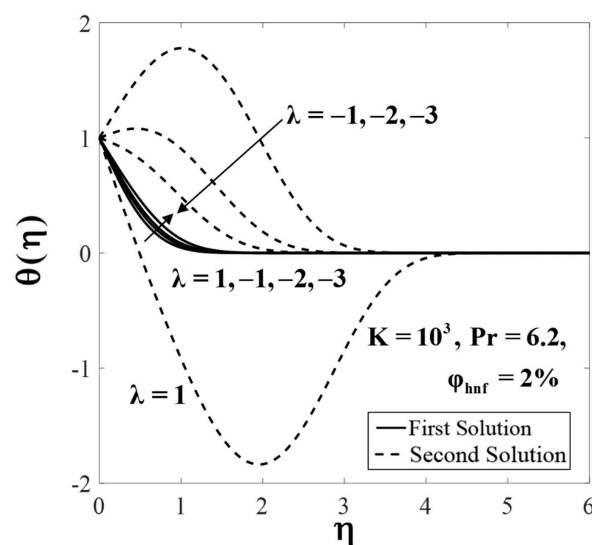**Figure 4.** Velocity profiles $f'(\eta)$ for different values of λ.

Figure 5. Temperature profiles $\theta(\eta)$ for different values of λ.
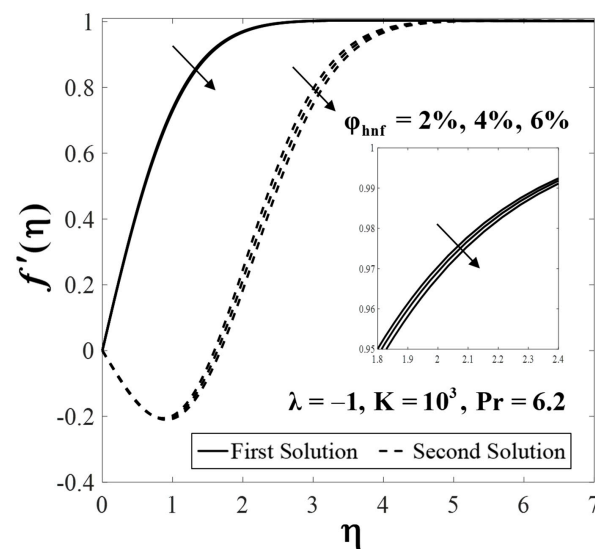
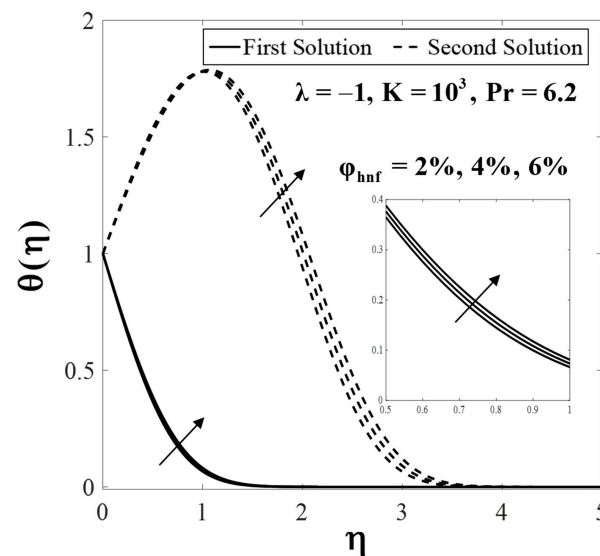**Figure 6.** Velocity profiles $f'(\eta)$ for different values of φ_{hnf}.

Figure 7. Temperature profiles $\theta(\eta)$ for different values of φ_{hnf}.

Furthermore, the dimensionless stream function is plotted to show the flow patterns. In this respect, the streamlines of the first and the second solutions for the opposing flow ($\lambda = -2$) when $\varphi_{hnf} = 2\%$, $K = 10^3$, and Pr = 6.2 are shown in Figures 8 and 9, respectively. The flow patterns for the first solution show that the fluid is moving away from the slot ($x = 0$) and acts as the normal stagnation point flow. Meanwhile, the flow is split into two regions for the second solution, i.e., upper and lower regions. The upper region has similar pattern with that of the first solution, whereas reverse flow is observed in the lower region.

The variations of the smallest eigenvalues γ against the mixed convection parameter λ when $\varphi_{hnf} = 2\%$, Pr = 6.2, and $K = 10^3$ are described in Figure 10. For the positive value of γ, it is noted that $e^{-\gamma\tau} \to 0$ as time evolves ($\tau \to \infty$). In the meantime, for the negative value of γ, $e^{-\gamma\tau} \to \infty$. These behaviors show that the first solution is physically reliable and stable over time.
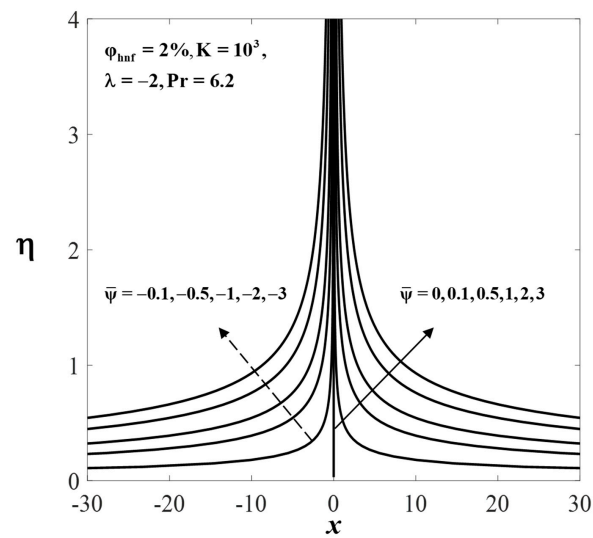
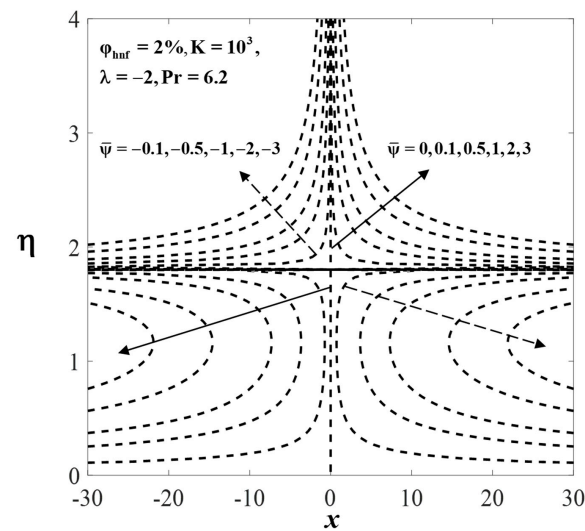**Figure 8.** Streamlines for the first solution.

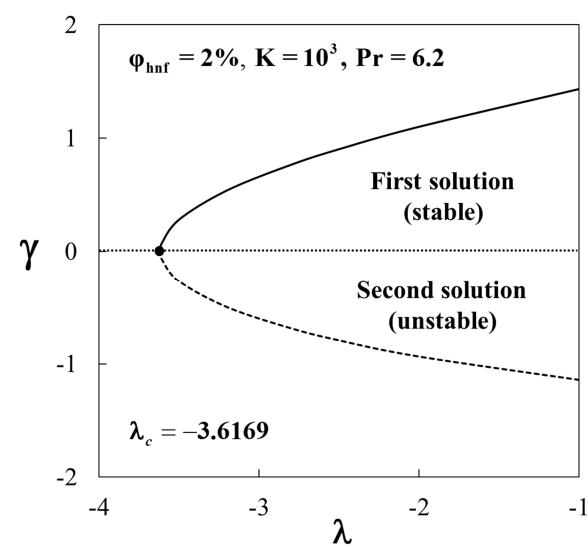**Figure 9.** Streamlines for the second solution.

Figure 10. Variation of the smallest eigenvalues γ against the mixed convection parameter λ.

6. Conclusions

In the present paper, the stagnation point flow towards a curved surface containing Al_2O_3-SiO_2 hybrid nanoparticles with buoyancy effects was accomplished. Findings revealed that dual solutions appeared for both assisting ($\lambda > 0$) and opposing ($\lambda < 0$) flows. The dual solutions were found for $\lambda > \lambda_c$ and no solution for $\lambda < \lambda_c$, while the solutions bifurcated at $\lambda = \lambda_c$. It was found that the critical values occur in the opposing flow region ($\lambda < 0$). The domain of the mixed convection parameter λ where the dual solutions are in existence increases as the percentage of φ_{hnf} is increased. Moreover, the higher percentage of φ_{hnf} gave rise to the heat transfer rate and the skin friction coefficient. Lastly, it was found that the first solution is stable and physically reliable as time evolves, while the second solution is not.

Author Contributions: Conceptualization, I.P.; funding acquisition, A.I.; methodology, I.W.; Project administration, A.I.; supervision, A.I. and I.P.; validation, I.P.; writing—original draft, I.W.; writing—review and editing, A.I., I.P. All authors have read and agreed to the published version of the manuscript.

Conflicts of Interest: The authors declare no conflict of interest.

References

1. Hiemenz, K. Die Grenzschicht an einem in den gleichförmigen Flüssigkeitsstrom eingetauchten geraden Kreiszylinder. *Dinglers Polytech. J.* **1911**, *326*, 321–410.
2. Homann, F. Der Einflub grober Zähigkeit bei der Strömung um den Zylinder und um die Kugel. *Z. für Angew. Math. und Mech.* **1936**, *16*, 153–164. [CrossRef]
3. Chiam, T.C. Stagnation-point flow towards a stretching plate. *J. Phys. Soc. Jpn.* **1994**, *63*, 2443–2444. [CrossRef]
4. Merkin, J.H. Mixed convection boundary layer flow on a vertical surface in a saturated porous medium. *J. Eng. Math.* **1980**, *14*, 301–313. [CrossRef]
5. Ishak, A.; Nazar, R.; Arifin, N.M.; Pop, I. Dual solutions in mixed convection flow near a stagnation point on a vertical porous plate. *Int. J. Therm. Sci.* **2008**, *47*, 417–422. [CrossRef]
6. Khashi'ie, N.S.; Arifin, N.M.; Rashidi, M.M.; Hafidzuddin, E.H.; Wahi, N. Magnetohydrodynamics (MHD) stagnation point flow past a shrinking/stretching surface with double stratification effect in a porous medium. *J. Therm. Anal. Calorim.* **2019**, *8*, 1–14. [CrossRef]
7. Dholey, S. An unsteady separated stagnation-point flow towards a rigid flat plate. *J. Fluids Eng.* **2019**, *141*, 021202. [CrossRef]
8. Fang, T.; Wang, F.; Gao, B. Unsteady magnetohydrodynamic stagnation point flow—closed-form analytical solutions. *Appl. Math. Mech.* **2019**, *40*, 449–464. [CrossRef]
9. Mahapatra, T.R.; Sidui, S. Non-axisymmetric Homann stagnation-point flow of a viscoelastic fluid towards a fixed plate. *Eur. J. Mech. B/Fluids* **2020**, *79*, 38–43. [CrossRef]
10. Weidman, P. Non-axisymmetric stagnation-point flow in a fluid saturated porous medium. *J. Porous Media* **2020**, *23*, 563–572. [CrossRef]
11. Kumar, B.; Seth, G.S.; Nandkeolyar, R. Quadratic multiple regression model and spectral relaxation approach to analyse stagnation point nanofluid flow with second-order slip. *Proc. Inst. Mech. Eng. Part E J. Process. Mech. Eng.* **2020**, *234*, 3–14. [CrossRef]
12. Choi, S.U.S.; Eastman, J.A. Enhancing thermal conductivity of fluids with nanoparticles. *Proc. 1995 ASME Int. Mech. Eng. Congr. Expo. FED 231/MD* **1995**, *66*, 99–105.
13. Khanafer, K.; Vafai, K.; Lightstone, M. Buoyancy-driven heat transfer enhancement in a two-dimensional enclosure utilizing nanofluids. *Int. J. Heat Mass Transf.* **2003**, *46*, 3639–3653. [CrossRef]
14. Tiwari, R.K.; Das, M.K. Heat transfer augmentation in a two-sided lid-driven differentially heated square cavity utilizing nanofluids. *Int. J. Heat Mass Transf.* **2007**, *50*, 2002–2018. [CrossRef]
15. Oztop, H.F.; Abu-Nada, E. Numerical study of natural convection in partially heated rectangular enclosures filled with nanofluids. *Int. J. Heat Fluid Flow* **2008**, *29*, 1326–1336. [CrossRef]
16. Hamad, M.A.A. Analytical solution of natural convection flow of a nanofluid over a linearly stretching sheet in the presence of magnetic field. *Int. Commun. Heat Mass Transf.* **2011**, *38*, 487–492. [CrossRef]
17. Kameswaran, P.K.; Narayana, M.; Sibanda, P.; Murthy, P.V.S.N. Hydromagnetic nanofluid flow due to a stretching or shrinking sheet with viscous dissipation and chemical reaction effects. *Int. J. Heat Mass Transf.* **2012**, *55*, 7587–7595. [CrossRef]

18. Khan, U.; Zaib, A.; Khan, I.; Nisar, K.S. Activation energy on MHD flow of titanium alloy (Ti6Al4V) nanoparticle along with a cross flow and streamwise direction with binary chemical reaction and non-linear radiation: Dual solutions. *J. Mater. Res. Technol.* **2020**, *9*, 188–199. [CrossRef]

19. Waini, I.; Ishak, A.; Pop, I. Dufour and Soret effects on Al_2O_3-water nanofluid flow over a moving thin needle: Tiwari and Das model. *Int. J. Numer. Methods Heat Fluid Flow* **2021**, *31*, 766–782. [CrossRef]

20. Majeed, A.; Zeeshan, A.; Hayat, T. Analysis of magnetic properties of nanoparticles due to applied magnetic dipole in aqueous medium with momentum slip condition. *Neural Comput. Appl.* **2019**, *31*, 189–197. [CrossRef]

21. Ghosh, S.; Mukhopadhyay, S. Stability analysis for model-based study of nanofluid flow over an exponentially shrinking permeable sheet in presence of slip. *Neural Comput. Appl.* **2020**, *32*, 7201–7211. [CrossRef]

22. Olayiwola, S.O.; Dejam, M. Experimental study on the viscosity behavior of silica nanofluids with different ions of electrolytes. *Ind. Eng. Chem. Res.* **2020**, *59*, 3575–3583. [CrossRef]

23. Bollineni, P.K.; Dordzie, G.; Olayiwola, S.O.; Dejam, M. An experimental investigation of the viscosity behavior of solutions of nanoparticles, surfactants, and electrolytes. *Phys. Fluids* **2021**, *33*, 026601. [CrossRef]

24. Sidik, N.A.C.; Adamu, I.M.; Jamil, M.M.; Kefayati, G.H.R.; Mamat, R.; Najafi, G. Recent progress on hybrid nanofluids in heat transfer applications: A comprehensive review. *Int. Commun. Heat Mass Transf.* **2016**, *78*, 68–79. [CrossRef]

25. Turcu, R.; Darabont, A.; Nan, A.; Aldea, N.; Macovei, D.; Bica, D.; Vekas, L.; Pana, O.; Soran, M.L.; Koos, A.A.; et al. New polypyrrole-multiwall carbon nanotubes hybrid materials. *J. Optoelectron. Adv. Mater.* **2006**, *8*, 643–647.

26. Jana, S.; Salehi-Khojin, A.; Zhong, W.H. Enhancement of fluid thermal conductivity by the addition of single and hybrid nano-additives. *Thermochim. Acta* **2007**, *462*, 45–55. [CrossRef]

27. Suresh, S.; Venkitaraj, K.P.; Selvakumar, P.; Chandrasekar, M. Synthesis of Al_2O_3-Cu/water hybrid nanofluids using two step method and its thermo physical properties. *Colloids Surf. A Physicochem. Eng. Asp.* **2011**, *388*, 41–48. [CrossRef]

28. Singh, S.K.; Sarkar, J. Energy, exergy and economic assessments of shell and tube condenser using hybrid nanofluid as coolant. *Int. Commun. Heat Mass Transf.* **2018**, *98*, 41–48. [CrossRef]

29. Farhana, K.; Kadirgama, K.; Rahman, M.M.; Noor, M.M.; Ramasamy, D.; Samykano, M.; Najafi, G.; Sidik, N.A.C.; Tarlochan, F. Significance of alumina in nanofluid technology: An overview. *J. Therm. Anal. Calorim.* **2019**, *138*, 1107–1126. [CrossRef]

30. Takabi, B.; Salehi, S. Augmentation of the heat transfer performance of a sinusoidal corrugated enclosure by employing hybrid nanofluid. *Adv. Mech. Eng.* **2014**, *6*, 147059. [CrossRef]

31. Kumar, V.; Sarkar, J. Particle ratio optimization of Al_2O_3-MWCNT hybrid nanofluid in minichannel heat sink for best hydrothermal performance. *Appl. Therm. Eng.* **2020**, *165*, 114546. [CrossRef]

32. Salehi, S.; Nori, A.; Hosseinzadeh, K.; Ganji, D.D. Hydrothermal analysis of MHD squeezing mixture fluid suspended by hybrid nanoparticles between two parallel plates. *Case Stud. Therm. Eng.* **2020**, *21*, 100650. [CrossRef]

33. Muhammad, K.; Hayat, T.; Alsaedi, A.; Ahmad, B. Melting heat transfer in squeezing flow of basefluid (water), nanofluid (CNTs + water) and hybrid nanofluid (CNTs + CuO + water). *J. Therm. Anal. Calorim.* **2021**, *143*, 1157–1174. [CrossRef]

34. Waini, I.; Ishak, A.; Pop, I. Hybrid nanofluid flow over a permeable non-isothermal shrinking surface. *Mathematics* **2021**, *9*, 538. [CrossRef]

35. Khan, U.; Waini, I.; Ishak, A.; Pop, I. Unsteady hybrid nanofluid flow over a radially permeable shrinking/stretching surface. *J. Mol. Liq.* **2021**, *331*, 115752. [CrossRef]

36. Sarkar, J.; Ghosh, P.; Adil, A. A review on hybrid nanofluids: Recent research, development and applications. *Renew. Sustain. Energy Rev.* **2015**, *43*, 164–177. [CrossRef]

37. Babu, J.A.R.; Kumar, K.K.; Rao, S.S. State-of-art review on hybrid nanofluids. *Renew. Sustain. Energy Rev.* **2017**, *77*, 551–565. [CrossRef]

38. Sajid, M.U.; Ali, H.M. Thermal conductivity of hybrid nanofluids: A critical review. *Int. J. Heat Mass Transf.* **2018**, *126*, 211–234. [CrossRef]

39. Huminic, G.; Huminic, A. Entropy generation of nanofluid and hybrid nanofluid flow in thermal systems: A review. *J. Mol. Liq.* **2020**, *302*, 112533. [CrossRef]

40. Yang, L.; Ji, W.; Mao, M.; Huang, J. An updated review on the properties, fabrication and application of hybrid-nanofluids along with their environmental effects. *J. Clean. Prod.* **2020**, *257*, 120408. [CrossRef]

41. Sajid, M.; Ali, N.; Javed, T.; Abbas, Z. Stretching a curved surface in a viscous fluid. *Chin. Phys. Lett.* **2010**, *27*, 024703. [CrossRef]

42. Sajid, M.; Ali, N.; Abbas, Z.; Javed, T. Flow of a micropolar fluid over a curved stretching surface. *J. Eng. Phys. Thermophys.* **2011**, *84*, 864–871. [CrossRef]

43. Abbas, Z.; Naveed, M.; Sajid, M. Heat transfer analysis for stretching flow over a curved surface with magnetic field. *J. Eng. Thermophys.* **2013**, *22*, 337–345. [CrossRef]

44. Abbas, Z.; Naveed, M.; Sajid, M. Hydromagnetic slip flow of nanofluid over a curved stretching surface with heat generation and thermal radiation. *J. Mol. Liq.* **2016**, *215*, 756–762. [CrossRef]

45. Hayat, T.; Kiran, A.; Imtiaz, M.; Alsaedi, A. Hydromagnetic mixed convection flow of copper and silver water nanofluids due to a curved stretching sheet. *Results Phys.* **2016**, *6*, 904–910. [CrossRef]

46. Imtiaz, M.; Hayat, T.; Alsaedi, A. Convective flow of ferrofluid due to a curved stretching surface with homogeneous-heterogeneous reactions. *Powder Technol.* **2017**, *310*, 154–162. [CrossRef]

47. Saba, F.; Ahmed, N.; Hussain, S.; Khan, U.; Mohyud-Din, S.; Darus, M. Thermal analysis of nanofluid flow over a curved stretching surface suspended by carbon nanotubes with internal heat generation. *Appl. Sci.* **2018**, *8*, 395. [CrossRef]

48. Sanni, K.M.; Asghar, S.; Jalil, M.; Okechi, N.F. Flow of viscous fluid along a nonlinearly stretching curved surface. *Results Phys.* **2017**, *7*, 1–4. [CrossRef]

49. Hayat, T.; Saif, R.S.; Ellahi, R.; Muhammad, T.; Ahmad, B. Numerical study of boundary-layer flow due to a nonlinear curved stretching sheet with convective heat and mass conditions. *Results Phys.* **2017**, *7*, 2601–2606. [CrossRef]

50. Okechi, N.F.; Jalil, M.; Asghar, S. Flow of viscous fluid along an exponentially stretching curved surface. *Results Phys.* **2017**, *7*, 2851–2854. [CrossRef]

51. Saleh, S.H.M.; Arifin, N.M.; Nazar, R.; Pop, I. Unsteady micropolar fluid over a permeable curved stretching shrinking surface. *Math. Probl. Eng.* **2017**, *2017*, 3085249. [CrossRef]

52. Naveed, M.; Abbas, Z.; Sajid, M.; Hasnain, J. Dual solutions in hydromagnetic viscous fluid flow past a shrinking curved surface. *Arab. J. Sci. Eng.* **2018**, *43*, 1189–1194. [CrossRef]

53. Khan, M.R.; Pan, K.; Khan, A.U.; Nadeem, S. Dual solutions for mixed convection flow of $SiO_2 - Al_2O_3$/water hybrid nanofluid near the stagnation point over a curved surface. *Phys. A Stat. Mech. its Appl.* **2020**, *547*, 123959. [CrossRef]

54. Lok, Y.Y.; Amin, N.; Campean, D.; Pop, I. Steady mixed convection flow of a micropolar fluid near the stagnation point on a vertical surface. *Int. J. Numer. Methods Heat Fluid Flow* **2005**, *15*, 654–670. [CrossRef]

55. Merkin, J.H. On dual solutions occurring in mixed convection in a porous medium. *J. Eng. Math.* **1986**, *20*, 171–179. [CrossRef]

56. Weidman, P.D.; Kubitschek, D.G.; Davis, A.M.J. The effect of transpiration on self-similar boundary layer flow over moving surfaces. *Int. J. Eng. Sci.* **2006**, *44*, 730–737. [CrossRef]

57. Shampine, L.F.; Gladwell, I.; Thompson, S. *Solving ODEs with MATLAB*; Cambridge University Press: Cambridge, UK, 2003.